Functionalizing Gold Nanoparticles with Calix[4]arenes Monolayers for Enhancing Selectivity and Stability in ORR Electrocatalysis

Quentin Lenne, Alice Mattiuzzi, Ivan Jabin, Nicolas Le Poul, Corinne Lagrost, Yann Leroux

Functionalizing Gold Nanoparticles with Calix[4]arenes Monolayers for Enhancing Selectivity and Stability in ORR Electrocatalysis

Quentin Lenne, Alice Mattiuzzi, Ivan Jabin, Nicolas Le Poul, Yann R. Leroux, Corinne Lagrost**

Q. Lenne, Dr. Y.R. Leroux, Dr. C. Lagrost
Univ Rennes, CNRS, ISCR – UMR 6226, 35000 Rennes, France
E-mail: yann.leroux@univ-rennes1.fr, corinne.lagrost@univ-rennes1.fr

Dr. A. Matiuzzi
X4C, 48 rue Auguste Piccard, 6041 Gosselies, Belgium

Prof. I. Jabin
Laboratoire de Chimie Organique, Université libre de Bruxelles (ULB), CP 160/06, avenue F.D. Roosevelt 50, 1050 Brussels, Belgium

Dr. N. Le Poul
CEMCA, CNRS UMR 6521, Université de Bretagne Occidentale, 6 avenue Le Gorgeu, CS 93837, 29238 Brest, France

Keywords: surface functionalization, electrocatalysis, gold nanoparticle, diazonium, oxygen reduction reaction

Abstract: The deliberate surface modification of nanocatalysts with organic ligands has recently emerged as a promising strategy to boost their efficiency, durability and/or selectivity in key electrocatalytic processes. The interface between the metallic interface and the immobilized ligands promotes high electrocatalytic activity. Herein, the oxygen reduction reaction activity of gold nanoparticles functionalized with a covalently-bound monolayer of calix[4]arenes is compared with commercially available gold nanoparticles, classically stabilized through electrostatic adsorption of citrates onto the gold surfaces. Nanocatalysts coated by calix[4]arenes show enhanced selectivity and stability compared to their citrate-stabilized counterparts. These nanohybrids exhibit excellent activity with a dominant 4-electron reduction of O_2 with good electrocatalytic performances along with a high robustness under operation as revealed by X-ray photoelectrons spectroscopy analyses.

1. Introduction

Organic ligands or capping agents are traditionally employed for preparing metallic nanoparticles (NPs) with controlled shape and size in wet chemistry.[1-4] Their roles are to prevent the aggregation of nanoparticles in solution and to control their growth at the crystallographic level.[4] For applications in electrocatalysis, the ligands are considered as poisonous species, blocking an important proportion of their active sites and deactivating the catalysts. The removal of ligands from the nanoparticles surface without altering the specific structure that rules their catalytic function, is a major challenge.[5-7]. Interestingly, organic ligands are commonly designed and employed in homogeneous catalysis to steer the activity and selectivity of metal centers.[8,9] The presence of organic ligands allows better control of selectivity. In line with this concept, the chemical surface modification of metallic nanostructures has just emerged as a promising strategy to increase their catalytic performances as recently reviewed.[10] Recent reports have highlighted that organic functionalization of metallic nanoparticles can boost their electrocatalytic properties through local interfacial steric or electronic effects.[11,12] Far from having a detrimental impact, the ligands are found to have a beneficial role. The nature of the ligands,[13] and/or the interfacial bonding,[14] promote high electrocatalytic activity, selectivity and durability.[10] The immobilization of organic molecules to metallic surfaces includes the chemisorption of monomers, polymers or surfactants, the self-assembly, the covalent grafting or the electrostatic adsorption of charged molecules (e.g. citrates, polyelectrolytes). The strength of interaction between surface and ligands depends on the employed procedures. Whereas thiol molecules are known for decades to efficiently bind gold nanoparticles (AuNPs) via Au-S bonds,[15,16] more recently, Au=C (carbene),[17] Au-C≡C (acetylide),[18] or Au-C (through aryl diazonium salts reduction),[19] provide robust interfacial bonds with strong metal-ligands interactions. The aryldiazonium reduction leads to strong interaction between the metallic surfaces and the aryl moieties, with adsorption energies over 200 $kJ.mol^{-1}$.[20] In contrast, electrostatic adsorption, involved for

instance in citrate-stabilized gold nanoparticles corresponds to a weaker interaction with binding energy lower than 85 kJ.mol^{-1}.[21]

We have recently developed a unique strategy to prepare dense and compact monolayers on a wide range of materials including nanomaterials thanks to the reductive grafting of calix[4]arene-tetradiazonium salts.[22,23] The calix[4]arene-tetradiazonium cation exhibits a cone-constrained structure made up of four aromatic units linked by methylene bridges, allowing a clean control of the formation of robust monolayers.[24] The large rim is equipped with four reactive diazonium functions, hence providing multiple anchoring points.[24] Such a multidentate structure enhances the stability and the organization of the monolayer, similar to what was described in the literature with other multidentate anchoring systems.[25] Importantly, we demonstrate that gold nanoparticles functionalized with calix[4]arene-tetradiazonium salts have exceptional colloidal robustness toward halides or extreme pH.[26]

Such a property is potentially very appealing for applications in electrocatalysis, notably for oxygen reduction reaction (ORR) since the experimental conditions are demanding. ORR is one of the most important electrochemical reaction in energy conversion technologies, e.g. electrocatalytic water splitting,[27,28] metal-air batteries [29,30] and fuel cells.[31,32] The cathodic oxygen reduction reaction is a slow multielectronic reaction which therefore occurs at high overpotential in the absence of a suitable catalyst. The 4-electron reduction process is generally desired and produces water. Platinum and platinum-based alloys are still the best ORR catalysts for proton exchange membrane fuel cells (PEMFCs) operating under acidic conditions[5,6,33-35] although, breakthroughs have been recently achieved with non-noble metals electrocatalysts.[30,36] Alkaline fuel cells could represent an alternative technology for which gold, silver and metal oxides are even better catalysts than Pt.[37-41] Moreover, anions, which are possible poisonous species, undergo lower adsorption energies in alkaline media than in acid ones.[42] In this context, AuNPs efficiently catalyze ORR, mainly through an indirect 4e- (2+2 e-) pathway.[37,38,41]

Herein, we present the electrocatalytic activity toward ORR of AuNPs functionalized with a covalently-bound monolayer of calix[4]arenes (i.e. Calix-AuNPs). The monolayer allows well-organized structure with a fine molecular control of distribution of ligands. So far, the effect of a well-organized and robust structure on the ORR properties of the modified AuNPs have not yet been explored. Especially, the fine control of ligands distribution on AuNPs surfaces remains highly challenging. In addition, the rigid structure of calix[4]arenes moieties allows a fine spatial control of the small rim substituents which is imposed by the small rim geometry. Thus the acetic acid arms are perfectly positioned at the solid/liquid interface, able to modulate the interaction between electrolyte and the catalytic surface. The electrocatalytic performance of the calix-AuNPs is compared to AuNPs modified with citrates (i.e., Citrate-AuNPs) (**Figure 1**). Recent works have indeed reported the good activity of citrates-capped AuNPs of 15 nm size as electrocatatalysts for ORR.[13,43] Citrates are the most classical ligands used for commercially available AuNPs. They stabilize AuNPs through electrostatic adsorption by forming multilayers in a disordered arrangement.[44] The interaction between metallic catalysts and ligands in citrate-AuNPs is then basically different from that involved in calix-AuNPs, making the comparison of the two materials attractive. The results are discussed in terms of nanohybrids efficiency and stability as well as mechanistic pathway for ORR.

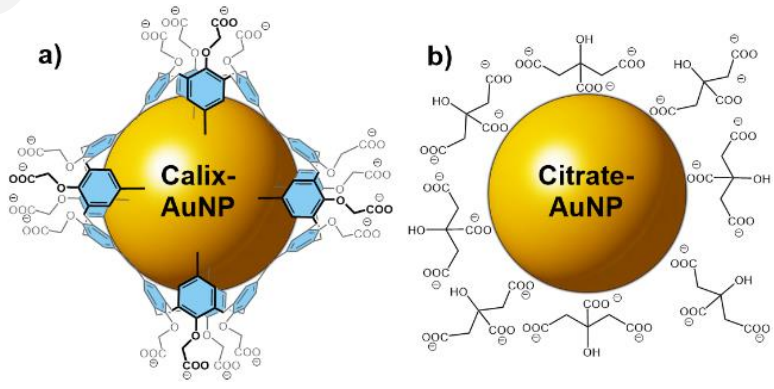

Figure 1. Schematic representation of (a) AuNPs functionalized with calix[4]arenes (calix-AuNPs) and (b) AuNPs stabilized with citrates (citrate-AuNPs).

2. Results and Discussion

Gold nanoparticles functionalized by calixarenes through diazonium reduction were synthesized as previously described.[26] Briefly, a solution of $HAuCl_4$ is reduced in the presence of calix[4]arene-tetraacetic acid-tetradiazonium salts via the addition of $NaBH_4$ to yield calix[4]arene-functionalized AuNPs (i.e. calix-AuNPs) of 6.1 ± 1.9 nm. Upon addition of the reducing agent in the solution, aurate salts and aryl diazoniums are transformed to gold clusters and aryl radicals, respectively. The aryl radicals are able to react with the gold surface forming a strong bond between the calix[4]arenes molecules and the gold nanoparticles. Because of the constrained macrocyclic structure of the calix[4]arene, the nanoparticles are covered with a monolayer of calixarenes as previously demonstrated.[24,26] Growth of nanoparticles is presumably stopped by the grafting of calix[4]arene-based radicals. **Figure 2** shows the particle size distribution after a simple centrifugation step. A good size dispersity is obtained for the functionalized calix-AuNPs with a primary size of 6.1 nm.

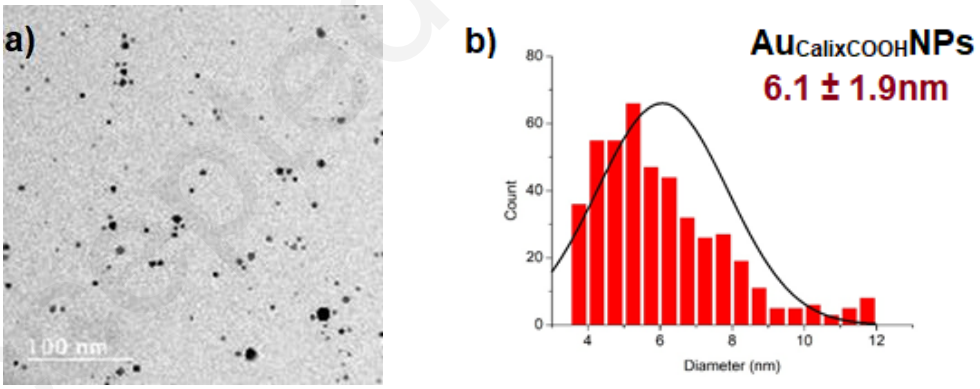

Figure 2. a) TEM micrographs and b) corresponding particle core size histogram of calix-AuNPs.

Taking into account that the size of the AuNPs has a drastic impact on their electrocatalytic activity that increases as nanoparticle size decreases,[43,45] it is necessary to work with citrate-AuNPs and calix-AuNPs with close size. Consequently, citrate-AuNPs of 5 ± 1 nm will be used in the following.

The ORR electrocatalytic activities of the two surface-modified AuNPs have been measured using a platinum ring (Pt)/glassy carbon disk (GC) rotating ring-disk electrode (RRDE) in O_2-saturated aqueous 0.1 M KOH, after deposition of AuNPs onto the GC disk surface (**Figure 3**). In alkaline solutions, oxygen (O_2) can be reduced to hydroxide anions (OH^-) by a direct 4-electron pathway:[46]

$O_2 + 2\ H_2O + 4\ e^- \rightarrow 4\ OH^-$; E° = 0.401 V vs. SHE

or it can follow an indirect 2 + 2 electrons pathway where O_2 is first reduced to hydroperoxide ion:[46]

$O_2 + H_2O + 2\ e^- \rightarrow HO_2^- + OH^-$; E° = -0.076 V vs. SHE

which is then further reduced to hydroxide anions in a second step:

$HO_2^- + H_2O + 2\ e^- \rightarrow 3\ OH^-$; E° = 0.878 V vs. SHE

or by disproportionation:

$2\ HO_2^- \rightarrow 2\ OH^- + O_2$

The ORR onset potential of calix- and citrate- AuNPs are both close to 0.90 V vs. RHE, corresponding to 330 mV and 270 mV overpotential values, respectively (Figure S4, Supporting Information). Half-wave potentials were determined as 0.80 and 0.83 V vs. RHE, respectively. Such values are comparable to those displayed by commercial Pt/C catalysts,[47-49] and other metallic electrocatalysts[50,51] and are even significantly more positive than other AuNPs-based catalysts (Table S2, Supporting Information).[52,53] In addition, this observation does show efficient electrocatalytic activity in ORR despite the capping of the metal cores, especially in the case of a robust capping as with the covalently-bound calix[4]arenes onto AuNPs surface. The amount of hydroperoxide ions (HO_2^-) generated during ORR at the GC disk was monitored by collection experiments at the Pt ring electrode which was set to a potential of +1.70 V (vs. RHE) to promote hydroperoxide oxidation (Figure 3, top curves). It is clear from Figure 3a that

almost no hydroperoxide ions are produced during ORR with calix-AuNPs whereas it can be clearly detected for citrate-AuNPs (Figure 3b).

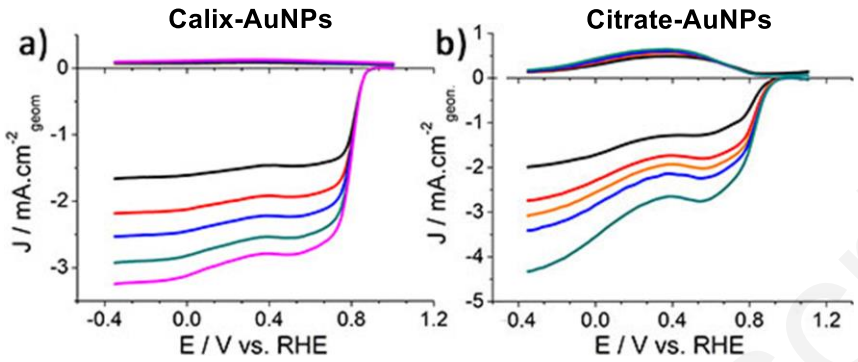

Figure 3. RRDE voltammetric curves in O_2-saturated 0.1 M KOH of GC disk electrodes modified with either (a) calix-AuNPs or (b) commercial citrate-AuNPs (bottom curves). Ring electrode (top curves): Pt. v = 10 mV.s^{-1}, 200 rpm < ω < 2000 rpm, E_{ring} = 1.70 V vs RHE.

From RRDE experiments, the number of electrons transferred per O_2 molecule (*n*) and the proportion of HO_2^- anions produced (% HO_2^-) can be determined. **Figure 4** displays the variation of *n* and % HO_2^- as a function of the potential during ORR (see Experimental Section for details). Very different behaviors are observed for calix- and citrate- AuNPs. With citrate-AuNPs, the process exhibits a variation of *n* values from 3.25 to 3.8 over the potential range (+0.8 V to -0.4 V vs RHE) (Figure 4a). The variation of *n* is correlated to the production of HO_2^- whose proportion varies between 5 to 30 % (Figure 4b). At high overpotentials, *n* decreases to 3.25 and this value corresponds to the maximum of HO_2^- production (at +0.4 V vs. RHE), in agreement with the shape of the LSV curves displayed in Figure 3b (bottom). This indicates that HO_2^- is formed as intermediate reduction product and is further reduced at more negative potentials, reaching an overall 4e- ORR process below -0.2 V vs. RHE (Figure 4). Hence, the reduction of O_2 at citrate-AuNPs proceeds through a stepwise 2e- + 2e- pathway. In sharp contrast, calix-AuNPs show a constant *n* value of 3.9 over the entire potential range along with a very low level (< 5%) of HO_2^- detected (Figure 4b, red curve). Such a result is very

interesting and quite unique for Au electrocatalysts.[13,43,52-57] Worth mentioning is that a stepwise 2e- +2e- process is generally observed with gold nanocatalysts in alkaline media as seen with citrate-AuNPs. Two-wave polarisation curves are generally obtained where HO_2^- is formed at the potential at the first wave, then can further undergo a complete reduction to OH^- at more negative potentials thanks to the good disproportionation activity of gold nanomaterials.[41,52] Bulk gold displays poor HO_2^- disproportionation activity and then predominantly reduce O_2 with 2 electrons. Only some Au single crystals Au(100) show exceptional catalytic $4e^-$ activity with almost no HO_2^- detection at low overpotentials but in a limited potential range.[58] Interestingly, carbon nanotubes- amphiphilic nitrilotriacetic-dyine lipid-gold nanohybrids catalysts were recently found to allow a predominant 4e- ORR process and low production of HO_2^- (< 10 %) in alkaline solution but in a limited potential range, close to the onset potential.[59] However, a very efficient disproportionation activity of this nanohybrid material was evidenced in the whole potential range [1; 0 V vs RHE].[59] Because the calix-AuNPs display « apparent» direct 4-e- process on the whole potential range with a very low HO_2^- formation (< 5%) and almost no variation of the number of electron exchanged (4), they exhibit enhanced selectivity towards the 4 e- process, close to what it is obtained with Pt electrocatalysts in acidic media. either through a direct 4e- process or a superior HO_2^- disproportionation.

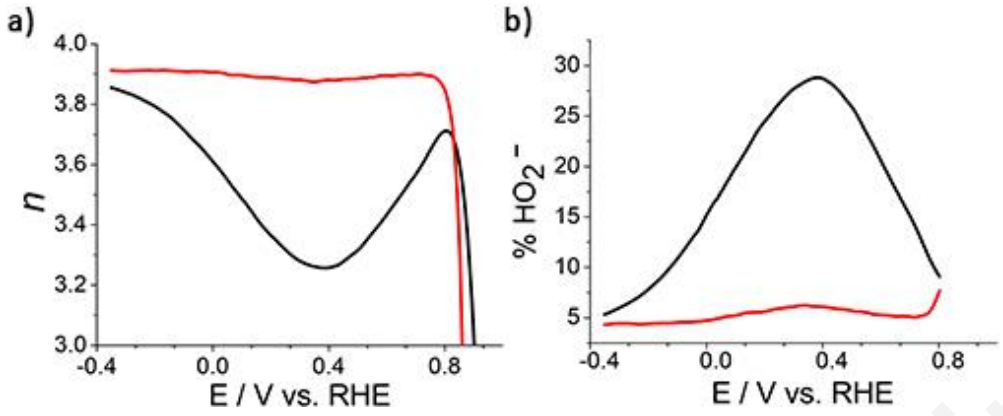

Figure 4. Potential dependence of (a) the number of electrons, n, and (b) the proportion of HO_2^- (% HO_2^-) produced during ORR experiments for calix-AuNPs (red lines) and citrate-AuNPs (black lines).

The kinetic current density (J_K) corresponds to the intrinsic activity of the catalysts and allows a quantification of their performance. J_K is further evaluated by using the Koutecký-Levich equation in the RDE voltammetric experiments to correct from mass-transfer contribution:

$$\frac{1}{J} = \frac{1}{J_K} + \frac{1}{J_L} = \frac{1}{J_K} + \frac{\omega^{-1/2}}{B} \qquad \text{(Equation 1)}$$

$$B = 0.62\, nFC_{O_2} D_{O_2}^{2/3} \nu^{-1/6} \qquad \text{(Equation 2)}$$

where J_L is the diffusion-limiting current density, n the overall number of electrons transferred during ORR, F the Faraday constant (96 485 C.mol^{-1}), C_{O2} the saturated O_2 concentration in the electrolyte (1.2 10^{-3} mol.L^{-1}), [56] D_{O2} the diffusion coefficient of O_2 in the electrolyte (1.9 10^{-5} cm².s^{-1}), [56] ν the kinematic viscosity of the solution (0.01 cm².s-1) and ω is the angular frequency (in rad.s^{-1}). Both series of AuNPs show good linearity of the Koutecký-Levich plots which demonstrates first-order reaction kinetics toward dissolved oxygen (Figure S5, Supporting Information). At +0.75 V vs. RHE, the normalized kinetic current density (per electrochemically active surface area, see Supporting Information), $J_{K,sp}$ was found equal to

1.22 and 2.73 mA.cm^{-2} for calix- and citrate-AuNPs, respectively. These values demonstrate good to very good performances of the two series of AuNPs compared to already reported specific activities of various metallic electrocatalysts including bare Pt and Au nanomaterials (see Table S2).

For both series of AuNPs, the mass-transfer corrected Tafel plots display two linear segments of different slopes (**Figure 5**). Such a change of the slopes is classically reported for ORR processes in both alkaline and acidic media (Table S2, Supporting Information). At low current density, we found absolute slopes equal to 42 mV/decade and 54 mV/decade for calix- and citrate-AuNPs, respectively. In the higher current density region, the corresponding absolute Tafel slopes were 124 mV/decade and 104 mV/decade, respectively (Figure 5). These values are rather close to the typical slopes of 60 mV/decade (low *J*) and 120 mV/decade (high *J*) generally found for ORR processes. It was shown that the former could correspond to a pseudo two-electrons transfer mechanism possibly involving the breaking of O-O bonds as the rate determining step.[60] At higher *J*, the rate-determining step was considered to be the first electron transfer.[61] One should note that microkinetic analyses are currently discussed and some authors have proposed that the change of the Tafel slope is not related to a change of rate-determining step but more likely due to the adsorption of species that could alter the kinetics.[62]

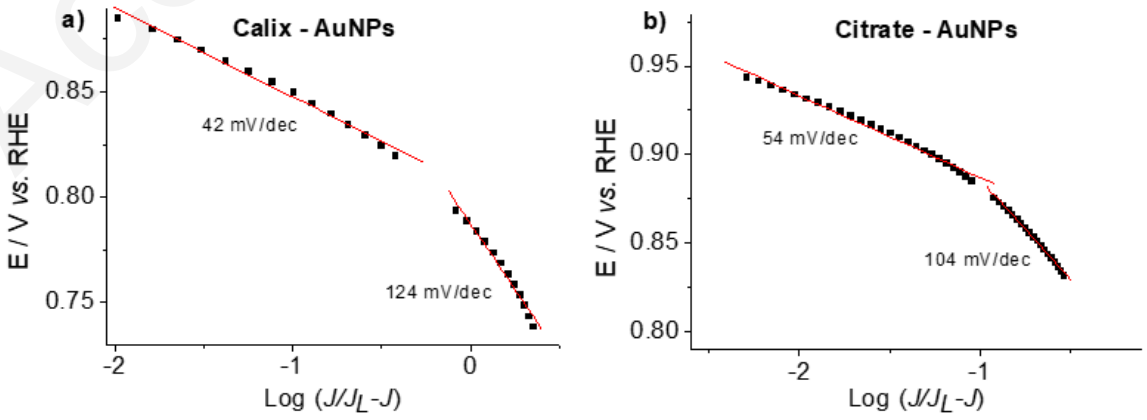

Figure 5. Mass-transfer corrected Tafel plots for O_2 reduction for (a) calix-AuNPs and (b) citrate-AuNPs in O_2-saturated aqueous 0.1 M KOH. v = 10 $mV.s^{-1}$; ω = 1600 rpm.

Interestingly, the absolute Tafel slope at low current density (42 mV/decade) for calix-AuNPs is significantly lower than the usual 60 mV/decade found for metal catalysts, showing the superior activity of calix-AuNPs. A similar value (43 mV/decade) has been reported for 5 nm bare Au nanoparticles.[56] A recent microkinetic modelling study has demonstrated that the *OOH + e- →*O + OH^- reaction (where *OOH and *O denote adsorbed transient species) could represent the rate determining step, leading to an absolute Tafel slope of 40 mV/decade.[61]

The two AuNPs hybrid systems show good stability upon long term chronoamperometry measurements at 0.75 V vs. RHE for 12 h in aqueous O_2-saturated 0.1 M KOH solution (Figure S6, Supporting Information). The calix-AuNPs have an even better stability than the citrate ones. Classically, the durability of ORR catalysts is probed through comparison of LSV curves before and after accelerated stability tests. They generally consist of one thousand cyclic voltammograms at 500 $mV.s^{-1}$ by sweeping the potentials between 1.2 V and – 0.35 V (vs. RHE) in O_2-saturated 0.1 M KOH solution. LSV curves were recorded after the accelerated stability tests and compared to the original ones (**Figure 6**). In line with the long term chronoamperometry measurements, the durability of calix-AuNPs and citrate-AuNPs are good, with a clear superior stability of calix-AuNPs compared to citrate-AuNPs. Almost no variation of the LSV curve is detected after the cycling process for calixarene nanohybrid catalyst.

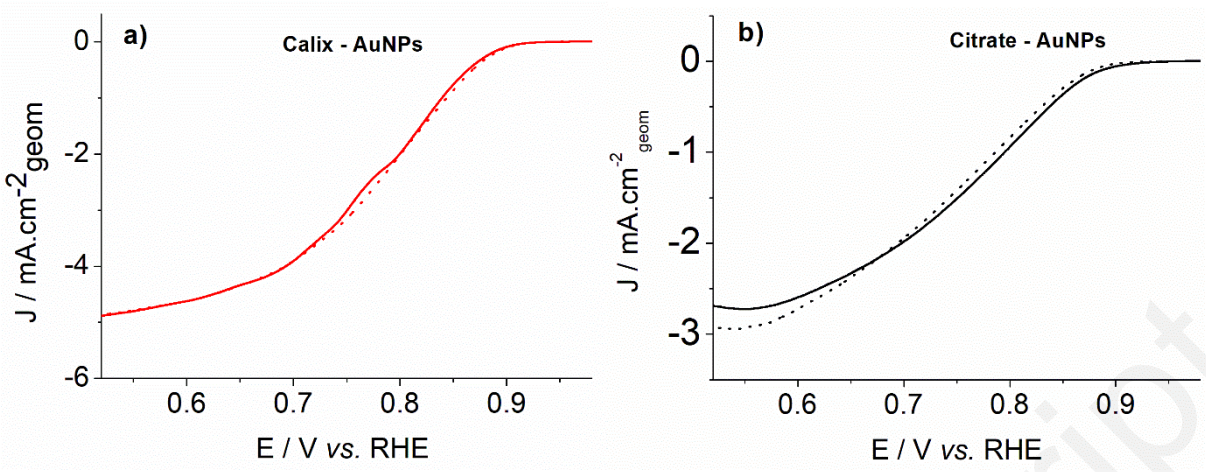

Figure 6. ORR polarization curves for calix-AuNPs (red curves) citrate-AuNPs (black curves) deposited onto the GC disk and recorded at room temperature in O_2-saturated aqueous 0.1 M KOH before (dotted curves) and after (solid line curves) accelerated stability tests. v= 10 mV s^{-1}. ω = 1600 rpm.

We performed a further study of the stability of the hybrid catalysts through measurements of electrochemically active surface area (ECSA) and X-ray photoelectron (XPS) spectra before and after accelerated stability tests. ECSA were estimated from cyclic voltammetries in acidic medium purged from O_2 through the integration of reduction peak of gold oxides (Figure S7, Supporting Information). While only 22% of citrate-AuNPs remains active after stability tests, 63% of calix-AuNPs is still operative. XPS analyses were performed before and after stability tests to evidence any possible change of the chemical composition after ORR experiments (**Figure 7**). High-resolution core level spectra in the C 1s region are peak-fitted and display several components (Figure 7). For Calix-AuNPs, a main peak centered at 284.5 eV could be mostly attributed to aliphatic and aromatic carbons of calix[4]arenes as well as possible contribution of the substrate itself (Figure 7a). Component at 286.0 ± 0.3 eV corresponds to the ether bonds (C-O-C) of the calix[4]arene core while the component at 289.1 ± 0.4 eV eV (O-C=O) is assigned to the carboxylic acid groups substituting the small rim of the calix[4]arene core. Two other components at 291.5 ± 0.2 eV (CF_2) and 293.2 ± 0.2 eV (CF_3) are due to the Nafion used in these experiments. Except a small erosion of Nafion coverage, the peak-fitted C

1s signal is fully comparable before and after ORR stability tests (Figure 7a,b). Especially, the component ratio COC/COOH is close to 1, i.e. 1.03 and 1.2 before and after ORR experiments, respectively (Table S1, Supporting Information). Such a value is in good agreement with the 1:1 ratio expected from the molecular structure of calix[4]arene. This observation indicates that there is no degradation of the hybrid calix-AuNPs catalysts during ORR.

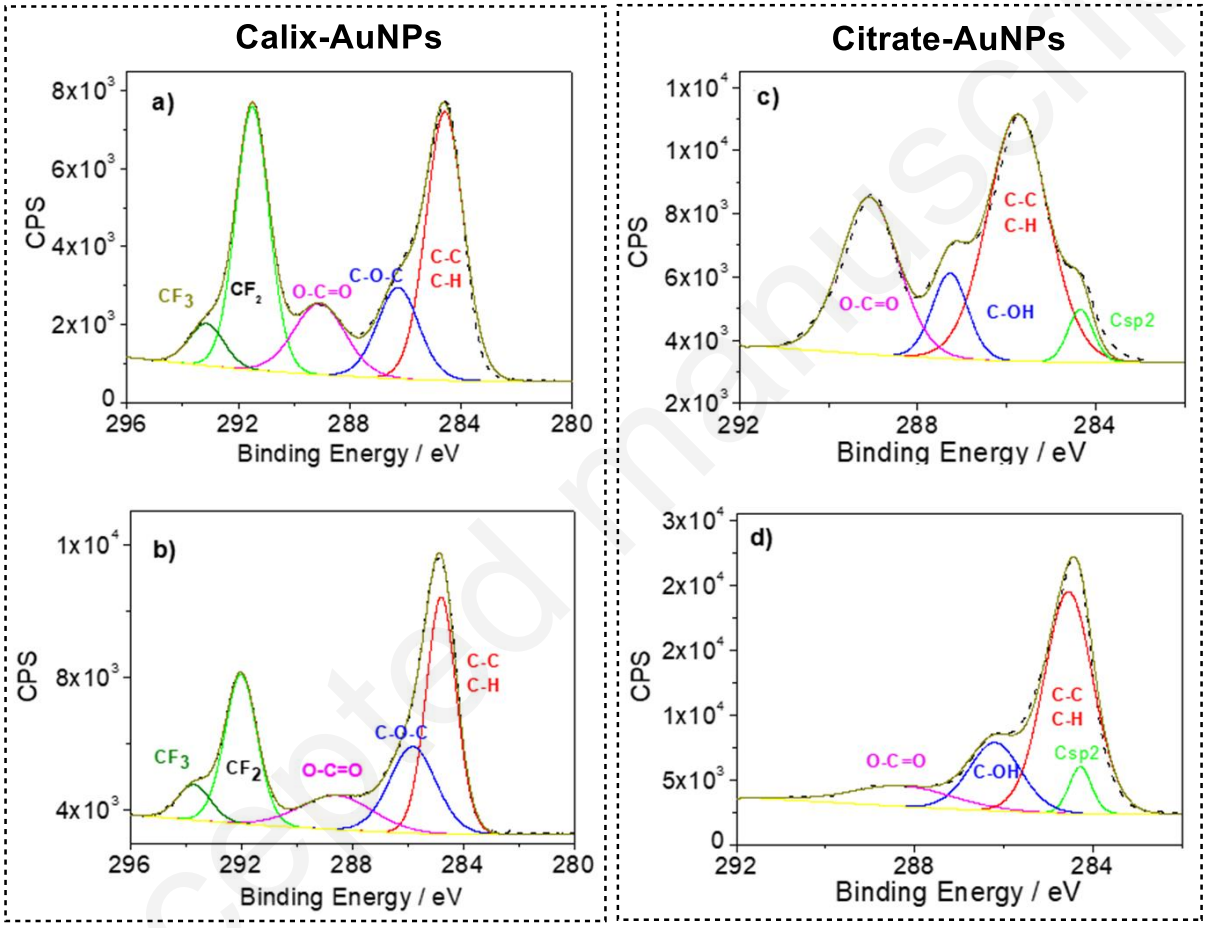

Figure 7. High-resolution XPS core level spectra of the C 1s region before a), c) and after b), d) ORR stability experiments on a), b) deposit of calix-AuNPs and c), d) citrate-AuNPs. The small contribution at 284.3 eV characteristic of C sp^2 carbon (c and d) is attributed to the carbon substrate. [63]

In sharp contrast, the chemical footprint of the citrate-AuNPs is totally different after stability experiments (Figures 7c, d and S9, Supporting Information). Before stability tests, peaks centered at 285.7 ± 0.3 eV (C-H/C-C), 287.2 ± 0.3 eV (C-OH) and 289.1 ± 0.3 eV (COO-) are identified in the high-resolution peak-fitted C1s core level spectra (Figure 7c). They correspond

to the chemical structure of the citrate ligands stabilizing the AuNPs as previously described.[44,64] The component ratio COOH/COH is found equal to 3 as expected from the molecular structure of citrate (Table S1, Supporting Information). After stability tests, a significant shift of the peak corresponding to C-C/C-H is observed along with a clear decrease of the C-OH and COO- components. The component ratio COOH/COH decreases to 1.7 (Table S1, Supporting Information). Thus, the XPS results suggest a chemical decomposition of the citrate molecules stabilizing the AuNPs. The loss of activity for the citrate-AuNPs is directly related to this chemical degradation. Upon degradation of their citrate shell, AuNPs are much prone to aggregation, explaining the dramatic decrease in ECSA measurements after stability test. It may be inferred from these observations that the active catalytic surface for citrate-AuNPs is actually the gold surface being rid of citrates molecules. Contrariwise, the monolayer of calix[4]arenes remains intact, suggesting that in case of calix-AuNPs, the whole nanohybrid system is active.

3. Conclusion

In summary, chemically modified gold nanoparticles (5 and 6 nm) with citrates and calix[4]arene-based organic ligands were shown to be efficient electrocatalysts for ORR in alkaline media. Electrochemical analyses clearly demonstrate that the calix[4]arene-functionalized AuNPs outperform on several points the citrate-AuNPs, despite a slightly larger size. This is ascribed to interfacial steric and electronic effect induced by the covalent functionalization of the AuNPs with monolayers of calix[4]arenes. The performances of the calix-AuNPs hybrid system are particularly interesting with a rather low overpotential and a predominant 4 e- ORR process, equaling Pt-based materials under similar conditions.[65] The stability of AuNPs under operation is significantly enhanced when they are functionalized with calix[4]arenes platform compared to citrates capping. The calix-AuNPs nanohybrids compare favorably with other reported AuNPs electrocatalysts (see also Table S2, Supporting

Information).[14,43,53-57] Such a robust electrocatalyst appears promising for application in fuel cells or O_2 sensors, and opens perspectives to expand the calixarene functionalization strategy toward other electrocatalytic reactions. Further works are currently under progress in order to tune the electrolyte/catalytic metal interface by modifying the small rim functions.

4. Experimental section

*Chemicals***.** Solvents and reagents for the syntheses were at least of reagent grade quality and were used without further purification. Citrate capped 5 nm AuNPs were purchased from Ted Pella, Inc (manufactured by BBI solutions, https://bbisolutions.com/eu/gold-nanoparticles-5nm.html).

Synthesis and characterization of functionalized nanoparticles. Calix[4]arene functionalized gold nanoparticles were synthesized according to an one-pot procedure. Gold salt $HAuCl_4.3H_2O$ purchased from Sigma Aldrich (>99.9%, 18 mg, 0.0457 mmol) was dissolved in dry acetonitrile (20 mL) and mixed with an acetonitrile solution (20 mL) of calix[4]arene-tetraacetic acid-tetradiazonium salts (Figure S2, Supporting Information). The calix[4]arene-tetraacetic acid-tetradiazonium salts were synthesized as previously reported.[24,26]

[Caution! Although we have not encountered any problem, it is noted that diazonium salts derivatives are potentially explosive and should be handled with appropriate precautions.]

The reaction mixture was stirred vigorously at 0°C under Ar and an aqueous solution of $NaBH_4$ (Sigma Aldrich, ≥98%, 0.5 mg in 1 mL) was added dropwise. The color of the reaction mixture changed from yellow to dark ruby. After 2 hours of vigorous stirring at room temperature, the reaction mixture was centrifuged at 10 000 rpm for 20 min, resulting in gold nanoparticles functionalized with calix[4]arenes ligands, calix-AuNPs (18 mg, 0.0236 mmol). Calix-AuNPs were washed by resuspension/precipitation in 1 M NaOH and 1 M HCl aqueous solution respectively. Finally, after removal of supernatant, milli-Q water (18.2 MΩ.cm) was added to

dilute ionic species. Samples were concentrated by centrifugation to obtain a 2 mg_{AuNPs}/mL concentration.

Transmission Electron Microscopy. Morphology and size distribution of the samples were investigated by high-resolution transmission electron microscopy (HRTEM), using a Jeol 2100 with an acceleration voltage of 200 kV on which the images were recorded on a GATAN Orius 200 CCD camera. The size distribution was estimated using ImageJ software, version 1.52a. Deposition homogeneity was inspected by scanning electron microscopy (SEM) on a Jeol JSM 7100 combined with an energy dispersive X-ray spectroscopy Oxford Instruments AZtecEnergy detector.

Electrochemical analyses. The ORR activity was evaluated using a rotating Pt/GC ring-disk electrode (37% collection efficiency) controlled by a MSR Rotator from Pine Research. The GC electrode preparation (deposit of catalysts) is fully described in the Supporting Information. The LSV scans were recorded using an Autolab PGSTAT302N potentiostat-galvanostat (Metrohm) equipped with a BIPOT module, in a conventional three-electrode electrochemical cell at a scan rate of 10 $mV.s^{-1}$ in a 0.1 M KOH solution saturated with O_2. A graphite rod and a Hg/HgO, NaOH (1 M) electrode were used as counter and reference electrodes, respectively. Voltammograms were recorded with the Metrohm Nova 1.11 software. The potentials were not corrected from iR-drop. The potentials are reported against the reversible hydrogen electrode according to E (RHE) = E (Hg/HgO) + 0.059 pH + 0.140. The preparation of the GC electrodes and its characterization (SEM) is fully described in SI.

The number of electrons exchanged can be quantified using the disk and ring currents according to:

$$n = \frac{4\, I_D}{I_D + (\frac{I_R}{N})}$$

where I_D is the modulus of the disk current, I_R is the ring current corresponding to the oxidation of HO_2^- and N is the collection efficiency. N was determined as 0.37 using the ferro/ferricyanide couple, in agreement with manufacturer indication.[66]

The fraction of HO_2^- that is produced in the reaction can be calculated from:

$$\% HO_2^- = 100 \frac{2\left(\frac{I_R}{N}\right)}{I_D + \left(\frac{I_R}{N}\right)}$$

The onset potential E_{onset} was determined on the LSV curves as the potential corresponding to 1/100 of I_L, I_L being the diffusion limiting current.

Surface of electrochemically active AuNPs (ECSA) was measured by cyclic voltammetry at 100 $mV.s^{-1}$ in an aqueous 0.1 M $HClO_4$ purged with Ar. A graphite rod and a SCE electrode, KCl (sat.) were used as the counter and reference electrode, respectively. Potential was swept until stabilization of the signal.

$$ECSA = \frac{Qoxides}{m \times C}$$

where Q_{oxides} is the charge integrated from the voltammetric peak corresponding to the reduction of gold oxides, m is the mass of gold deposited and C is the monolayer adsorption charge on Au (400 µC cm^{-2}).[67] ECSA was found to be 0.36 cm^2 (0.11 $cm^2 \mu g^{-1}_{Au}$) and 1.52 cm^2 (0.092 $cm^2 \mu g^{-1}_{Au}$) for citrate- and calix-AuNPs, respectively.

X-ray photoelectron spectroscopy measurements. XPS data have been collected by a Kratos Axis Nova spectrometer using the Al Kα X-ray source working at 1486.6 eV and using a spot size of 0.7 x 0.3 mm². Survey spectra (0-1000 eV) (Figure S7) were acquired with an analyzer pass energy of 160 eV (0.5 eV/step); high resolution spectra used a pass energy of 40 eV (0.1 eV/step). Binding energies were referenced to C1s peak at 285 eV or to Au $4f_{7/2}$ at 84 eV. The core level spectra were peak-fitted using the CasaXPS Software, Ltd. Version 2.3.18. U2 Tougaard was used as background. The peaks areas were normalized by the manufacturer-supplied sensitivity factor (S_{C1s} = 0.278, S_{F1s} = 1, S_{O1s} = 0.78, S_{S2p} = 0.668, S_{Au4f} = 6.25). Since the XPS measurements cannot be made with the RRDE electrodes due to their height, deposit

of AuNPs were performed onto screen-printed carbon electrode Dropsens®. The modified electrodes subsequently underwent ORR stability experiments (1000 cycles at 500mV.s^{-1} from 1.20V to -0.35V vs RHE) under the same experimental conditions used for ORR measurements with RRDE. Due to their good mechanical stability onto the carbon electrode, the deposit of citrate-AuNPs were not covered with Nafion, to avoid the screening effect of the Nafion film. For each sample, XPS spectra were recorded on three different locations, and we did not observe any difference.

Supporting Information
Supporting Information is available from the Wiley Online Library or from the author.

Acknowledgements
Q.L. thanks the French Ministry of Research for financial support. J. Hamon (Institut des Matériaux de Nantes, Nantes, France) is warmly thanked for his help in recording the X-ray photoelectrons spectra. The authors are grateful to L. Rault for the assistance in TEM experiments performed on THEMIS platform (CPER-FEDER 2007–2014) and to F. Gouttefangeas for SEM experiments performed on CMEBA platform (THEMIS/CMEBA, ScanMAT, UMS 2R011 University of Rennes 1-CNRS, Rennes, France).

Conflict of Interest
I. J. and C. L. are shareholders of X4C. I.J. is a consultant for X4C. All other authors declare that they have no conflict of interest.

REFERENCES
[1] J. Park, J. Joo, S. G. Kwon, Y. Jang, T. Hyeon. *Angew. Chem. Int. Ed.* **2007,** *46,* 4630.
[2] M.-A. Neouze, U. Schubert. *Monatsh. Chem.* **2008,** *139,* 183.
[3] A. Quintanilla, V. C. L. Butselaar-Orthlieb, C. Kwakernaak, W. G. Sloof, M. T. Kreutzer, F. Kapteijn. *Journal of Catalysis* **2010,** *271,* 104.
[4] A. R. Tao, S. Habas, P. Yang. *Small* **2008,** *4,* 310.
[5] G. Fu, K. Wu, J. Lin, Y. Tang, Y. Chen, Y. Zhou, T. Lu. *J. Phys. Chem. C* **2013,** *117,* 9826.
[6] D. Y. Chung, S. W. Jun, G. Yoon, S. G. Kwon, D. Y. Shin, P. Seo, J. M. Yoo, H. Shin, Y.-H. Chung, H. Kim, B. S. Mun, K.-S. Lee, N.-S. Lee, S. J. Yoo, D.-H. Lim, K. Kang, Y.-E. Sung, T. Hyeon. *J. Am. Chem. Soc.* **2015,** *137,* 15478.
[7] X.-Y. Lang, G.-F. Han, B.-B. Xiao, L. Gu, Z.-Z. Yang, Z. Wen, Y.-F. Zhu, M. Zhao, J.-C. Li, Q. Jiang. *Adv. Funct. Mat.* **2015,** *25,* 230.
[8] M. L. Pegis, C. F. Wise, D. J. Martin, J. M. Mayer. *Chem. Rev.* **2018,** *118,* 2340.

[9] B. Das, A. Thapper, S. Ott, S. B. Colbran. *Sustainable Energy Fuels* **2019,** *3*, 2159.
[10] Q. Lenne, Y. R. Leroux, C. Lagrost. *ChemElectroChem* **2020,** *7*, 2345.
[11] Y. Peng, B. Lu, N. Wang, L. Li, S. Chen. *Phys. Chem. Chem. Phys.* **2017,** *19*, 9336.
[12] J. Wang, F. Zhang, X. Kang, S. Chen. *Curr. Op. Electrochem.* **2019,** *13*, 40.
[13] D. Alba-Molina, A. R. Puente Santiago, J. J. Giner-Casares, E. Rodríguez-Castellón, M. T. Martín-Romero, L. Camacho, R. Luque, M. Cano. *J. Mat. Chem. A* **2019,** *7*, 20425.
[14] P. Hu, L. Chen, X. Kang, S. Chen. *Acc. Chem. Res.* **2016,** *49*, 2251.
[15] M. Brust, M. Walker, D. Bethell, D. J. Schiffrin, R. Whyman. *J. Chem. Soc., Chem. Commun.* **1994**, DOI:10.1039/C39940000801 10.1039/C39940000801, 801.
[16] M. Brust, J. Fink, D. Bethell, D. J. Schiffrin, C. Kiely. *J. Chem. Soc., Chem. Commun.* **1995**, DOI:10.1039/C39950001655 10.1039/C39950001655, 1655.
[17] A. V. Zhukhovitskiy, M. J. MacLeod, J. A. Johnson. *Chem. Rev.* **2015,** *115*, 11503.
[18] P. Maity, H. Tsunoyama, M. Yamauchi, S. Xie, T. Tsukuda. *J. Am. Chem. Soc.* **2011,** *133*, 20123.
[19] F. Mirkhalaf, J. Paprotny, D. J. Schiffrin. *J. Am. Chem. Soc.* **2006,** *128*, 7400.
[20] D.-e. Jiang, B. G. Sumpter, S. Dai. *J. Am. Chem. Soc.* **2006,** *128*, 6030.
[21] K. Müller-Dethlefs, P. Hobza. *Chem. Rev.* **2000,** *100*, 143.
[22] L. Troian-Gautier, A. Mattiuzzi, O. Reinaud, C. Lagrost, I. Jabin. *Org. Biomol. Chem.* **2020,** *18*, 3624.
[23] A. Mattiuzzi, Q. Lenne, J. Carvalho Padilha, L. Troian-Gautier, Y. Leroux, I. Jabin, C. Lagrost. *Front. Chem.* **2020**, DOI:10.3389/fchem.2020.00559 10.3389/fchem.2020.00559
[24] A. Mattiuzzi, I. Jabin, C. Mangeney, C. Roux, O. Reinaud, L. Santos, J.-F. Bergamini, P. Hapiot, C. Lagrost. *Nature Commun.* **2012,** *3*, 1130.
[25] Z.-Q. Li, J.-H. Tang, Y.-W. Zhong. *Chem. Asian J.* **2019,** *14*, 3119.
[26] L. Troian-Gautier, H. Valkenier, A. Mattiuzzi, I. Jabin, N. V. den Brande, B. V. Mele, J. Hubert, F. Reniers, G. Bruylants, C. Lagrost, Y. Leroux. *Chem. Commun.* **2016,** *52*, 10493.
[27] L. Han, S. Dong, E. Wang. *Adv. Mat.* **2016,** *28*, 9266.
[28] S. Anantharaj, S. R. Ede, K. Sakthikumar, K. Karthick, S. Mishra, S. Kundu. *ACS Catal.* **2016,** *6*, 8069.
[29] F. Cheng, J. Chen. *Chem. Soc. Rev.* **2012,** *41*, 2172.
[30] Z.-L. Wang, D. Xu, J.-J. Xu, X.-B. Zhang. *Chem. Soc. Rev.* **2014,** *43*, 7746.
[31] L. Carrette, K. A. Friedrich, U. Stimming. *Fuel Cells* **2001,** *1*, 5.
[32] M. K. Debe. *Nature* **2012,** *486*, 43.
[33] J. Greeley, I. E. L. Stephens, A. S. Bondarenko, T. P. Johansson, H. A. Hansen, T. F. Jaramillo, J. Rossmeisl, I. Chorkendorff, J. K. Nørskov. *Nature Chem.* **2009,** *1*, 552.
[34] J. Snyder, T. Fujita, M. W. Chen, J. Erlebacher. *Nature Mat.* **2010,** *9*, 904.
[35] M. Sharma, N. Jung, S. J. Yoo. *Chem. Mat.* **2018,** *30*, 2.
[36] Z. Chen, D. Higgins, A. Yu, L. Zhang, J. Zhang. *Energ. Environm. Sci.* **2011,** *4*, 3167.
[37] M. S. El- Deab, T. Ohsaka. *Electrochem. Commun.* **2002,** *4*, 288.
[38] M. S. El-Deab, T. Ohsaka. *Electrochim. Acta* **2002,** *47*, 4255.
[39] A. Qaseem, F. Chen, X. Wu, R. L. Johnston. *Catal. Sci. Technol.* **2016,** *6*, 3317.
[40] P. Quaino, N. B. Luque, R. Nazmutdinov, E. Santos, W. Schmickler. *Angew. Chem. Int. Ed.* **2012,** *51*, 12997.
[41] P. Rodriguez, M. T. M. Koper. *Phys. Chem. Chem. Phys.* **2014,** *16*, 13583.
[42] J. S. Spendelow, A. Wieckowski. *Phys. Chem. Chem. Phys.* **2007,** *9*, 2654.
[43] D. Alba-Molina, A. R. Puente Santiago, J. J. Giner-Casares, M. T. Martín-Romero, L. Camacho, R. Luque, M. Cano. *J. Phys. Chem. C* **2019,** *123*, 9807.
[44] J.-W. Park, J. S. Shumaker-Parry. *J. Am. Chem. Soc.* **2014,** *136*, 1907.

[45] L. Wang, Z. Tang, W. Yan, H. Yang, Q. Wang, S. Chen. *ACS Appl. Mat. Interf.* **2016,** *8*, 20635.
[46] X. Ge, A. Sumboja, D. Wuu, T. An, B. Li, F. W. T. Goh, T. S. A. Hor, Y. Zong, Z. Liu. *ACS Catal.* **2015,** *5*, 4643.
[47] G. He, Y. Song, K. Liu, A. Walter, S. Chen, S. Chen. *ACS Catal.* **2013,** *3*, 831.
[48] J. E. Newton, J. A. Preece, N. V. Rees, S. L. Horswell. *Phys. Chem. Chem. Phys.* **2014,** *16*, 11435.
[49] Z.-Y. Zhou, X. Kang, Y. Song, S. Chen. *Chem. Commun.* **2012,** *48*, 3391.
[50] K. Jukk, N. Kongi, L. Matisen, T. Kallio, K. Kontturi, K. Tammeveski. *Electrochim. Acta* **2014,** *137*, 206.
[51] L. Jiang, A. Hsu, D. Chu, R. Chen. *J. Electrochem. Soc.* **2009,** *156*, B643.
[52] H. Erikson, G. Jürmann, A. Sarapuu, R. J. Potter, K. Tammeveski. *Electrochim. Acta* **2009,** *54*, 7483.
[53] H. Yin, H. Tang, D. Wang, Y. Gao, Z. Tang. *ACS Nano* **2012,** *6*, 8288.
[54] W. Chen, S. Chen. *Angew. Chem. Int. Ed.* **2009,** *48*, 4386.
[55] M. Govindhan, A. Chen. *J. Power Sources* **2015,** *274*, 928.
[56] H. Erikson, A. Sarapuu, K. Tammeveski, J. Solla-Gullón, J. M. Feliu. *ChemElectroChem* **2014,** *1*, 1338.
[57] W. Tang, H. Lin, A. Kleiman-Shwarsctein, G. D. Stucky, E. W. McFarland. *J. Phys. Chem. C* **2008,** *112*, 10515.
[58] R. R. Adžić, S. Strbac, N. Anastasijević. *Materials Chemistry and Physics* **1989,** *22*, 349.
[59] A. Morozan, S. Donck, V. Artero, E. Gravel, E. Doris. *Nanoscale* **2015,** *7*, 17274.
[60] H. A. Hansen, V. Viswanathan, J. K. Nørskov. *J. Phys. Chem. C* **2014,** *118*, 6706.
[61] T. Shinagawa, A. T. Garcia-Esparza, K. Takanabe. *Sci. Rep.* **2015,** *5*, 13801.
[62] A. Holewinski, S. Linic. *J. Electrochem. Soc.* **2012,** *159*, H864.
[63] M. I. González-Sánchez, B. Gómez-Monedero, J. Agrisuelas, J. Iniesta, E. Valero. *Electrochem. Commun.* **2018,** *91*, 36.
[64] J. G. Mehtala, D. Y. Zemlyanov, J. P. Max, N. Kadasala, S. Zhao, A. Wei. *Langmuir* **2014,** *30*, 13727.
[65] N. R. Elezovic, V. R. Radmilovic, J. Kovac, B. M. Babic, L. M. Gaijic-Krstajic, N. V. Krstajic. *RSC Adv.* **2015,** *5*, 15923.
[66] E. Claude, T. Addou, J. M. Latour, P. Aldebert. *J. App. Electrochem.* **1998,** *28*, 57.
[67] B. Piela, P. K. Wrona. *J. Electroanal. Chem.* **1995,** *388*, 69.

TOC graphic

Designing a gold-calix[4]arene nanohybrids for enhancing selectivity and stability in ORR.